Germanium Quantum Dot Grätzel-Type Solar Cell

Jonathan Cardoso, Sarita Marom, Justin Mayer, Ritika Modi, Alessandro Podestà, Xiaobin Xie, Marijn A. van Huis, and Marcel Di Vece*

Solar cells fabricated from sustainable quantum dot materials are currently not commercially available, but ongoing research provides a steady increase in efficiency and stability of laboratory devices. In this work, the first germanium quantum dot solar cell made with a gas aggregation nanoparticle source is presented. UV–vis spectroscopy reveals quantum confinement, and the spectral response of the germanium quantum dot Grätzel-type solar cell confirms the presence of large and small band gap optical absorption due to a mix of particle sizes. Some of the particles are small enough to have substantial quantum confinement while others are so large that they have bulk-like properties. The efficiency of the germanium quantum dot solar cells is very low but could reach 1% if the formation of germanium oxide layers is avoided in future experiments. This first quantum dot solar cell made with a gas aggregation nanoparticle source demonstrates, as a proof of concept, the technological potential for research and applications combining the fields of photovoltaics and gas aggregation nanoparticle sources.

1. Introduction

Quantum dots are an interesting form of matter because their band gap is tunable via control over the size of the semiconductor particle, typically well below 10 nm,[1,2] due to quantum confinement.[3] The inspiration to use quantum dots in solar cells are the tandem or multi-junction cells in which more photons of different energy are harvested. Although tandem solar cells are commercially available and they indeed have a higher efficiency,[4] they are very expensive, leaving ample space for research toward economically viable materials, such as cheap quantum dots. These quantum dots[3,5] allow the use of a single cheap semiconductor in a tandem solar cell. Quantum dots of different size and therefore different band gaps could harvest different parts of the solar spectrum. Although commercial quantum dot solar cells based on sustainable materials such as Ge are currently not available,[6] in this work we demonstrate its potential. The quantum dot based emitting displays (QDOT)[7] demonstrate that this technology could become a commercial product in the near future.

Solar energy conversion to electricity in laboratory quantum dot solar cells remains too low (currently 12%[8]) and therefore requires fundamental improvements. One of the key factors is the efficient transport of charge carriers (electrons and holes) toward the opposing electrodes. The chemical properties of the quantum dot surface, the material between the quantum dots and the contact properties with the electrodes are all very important to obtain the best efficiency. A class of well-studied quantum dots are the Pb- or Cd-based chalcogenide family (e.g., PbS, PbSe, and CdTe QDs), which are conveniently produced and have promising optical and electronic properties,[9] however, these materials are also toxic, and development of solar cells based on more sustainable material solutions is highly desired.

Although new concepts and materials are intensively investigated to further increase solar cell efficiencies, silicon remains a very attractive photovoltaïc (PV) material. Silicon as quantum dot for solar cells may lead to enhanced device performance.[10] Silicon quantum dots, which are employed in a tandem cell have the potential to not only tune the band gap of silicon,[11] but for the smallest sizes, a direct band gap may also appear.[12] In principle, a direct band gap increases absorption as compared to the indirect band gap of bulk crystalline silicon.[13] However, small quantum dots have a low density of states which in turn reduces their optical absorption. Quantum confinement in silicon nanoparticles has been demonstrated by photoluminescence, which yielded a clear size dependence.[14–18] Another interesting property is the generation of multiple excitons, which was observed by step-like enhancement of the luminescence quantum yield,[19] which was even possible in adjacent silicon nanoparticles.[20]

The main reason why silicon quantum dots are not yet implemented in solar cells is the difficulty to produce high-quality silicon quantum dots both by physical and chemical methods. Some proof of principle silicon quantum dot solar cells have been developed, such as the silicon-rich silicon oxide or silicon carbide, in which nanoparticles are formed upon annealing whereby the silicon atoms aggregate to form particles.[21,22] However, these silicon nanoparticles have a large

J. Cardoso, S. Marom, J. Mayer, R. Modi, Prof. A. Podestà,
Prof. M. Di Vece
Interdisciplinary Centre for Nanostructured Materials and Interfaces
(CIMaINa) and Department of Physics "Aldo Pontremoli"
Università degli Studi di Milano
Via Celoria 16, 20133 Milan, Italy
E-mail: marcel.divece@unimi.it

Dr. X. Xie, Prof. M. A. van Huis
Soft Condensed Matter, Debye Institute for Nanomaterials Science
Utrecht University
Princetonplein 5, 3584 CC Utrecht, The Netherlands

The ORCID identification number(s) for the author(s) of this article can be found under https://doi.org/10.1002/pssa.201800570.

size distribution and are often separated by large distances, which hinders electrical conductance. The large size distribution will prevent accurate tuning of the band gap and forms exciton trapping centers.

The fabrication of mono disperse quantum dots with controllable separation distance is a prerequisite for successful application in a solar cell. In a recent publication by Di Vece,[23] the gas aggregation nanoparticle source has been proposed as a promising device to produce semiconductor quantum dots. In a recent work by Tang et al.,[24] silicon nanoparticles were fabricated with such a gas aggregation nanoparticle source. In this work, we fabricate nanoparticles of the other group IV semiconductor: germanium, which is a novelty on its own. Germanium has similar chemical properties as silicon, with the advantage that the band gap (0.66 eV at 300 K[25]) is much smaller and that the Bohr radius of germanium, the size at which quantum confinement sets in, is about 24 nm.[26] This very large Bohr radius makes it an excellent material to explore the quantum confinement and implement this in a solar cell. Moreover, the optical absorption cross-section of germanium is much higher than that of silicon,[27] which makes it ideally suitable for very thin film solar cells. In this work, the germanium quantum dots, as produced by the magnetron sputtering gas aggregation nanoparticle source, were deposited on one electrode of a Grätzel-type solar cell.[28] Although the efficiency of this germanium quantum dot solar cell remains to be improved, a proof of principle germanium quantum dot solar cell fabricated with a gas aggregation nanoparticle source opens up a new avenue for quantum dot solar cell research and is therefore of high-technological value.

2. Experimental Section

The germanium nanoparticles were deposited with a gas aggregation nanocluster source based on magnetron sputtering (NC200U-B Oxford Applied Research Ltd.)[29,30] on glass with ITO (80 nm) substrates (1 cm^2). For the deposition of nanoparticles, argon gas was used as both sputter and carrier gas inside the gas aggregation chamber with a flow rate of 15 sccm. The germanium target had a purity of 99.999% and the dopant concentration Sb $<0.06\,\mu g\,g^{-1}$. The magnetron DC power was $\approx$110 W for all samples and the aggregation length was varied between 30 and 60 mm.

The germanium nanoparticles were investigated with two transmission electron microscopes (TEM): 1) Philipps CM10 (FEI) electron-microscope operated at 80 kV and 2) FEI Talos F200X TEM operated at 200 kV and equipped with Super-X energy-dispersive X-ray spectrometry (EDX). The TEM micrographs were taken of germanium nanoparticles deposited for 1 min on holey a-C TEM grids keeping the deposition parameters identical to the parameters used for the nanocomposite samples which were deposited on ITO. The morphological characteristics of the electrode surfaces were determined by atomic force microscopy (AFM) using a Bioscope Catalyst AFM by Bruker operated in Tapping Mode in air, equipped with standard probes with radius below 10 nm. AFM raw images were flattened by subtracting a paraboloid in order to remove the scanner-induced bow and the sample tilt. A median

filter was applied to AFM images to remove high-frequency noise. UV–vis absorbance spectra of the samples were recorded with a commercial double beam Agilent Cary-100 spectrophotometer with a wavelength range from 190 to 900 nm and a wavelength resolution of 0.5 nm.

To construct the Grätzel-type solar cell,[28] a few nm thin gold layer was evaporated on an ITO substrate to function as the cathode. The ITO sample with germanium nanoparticles was placed against the gold layer with about a 0.5 mm gap in between. The two 1 cm^2 plates were held together by a small metal frame. A standard I$^-$/I$_3^-$ redox couple organic electrolyte was used between the two electrodes to accommodate the regeneration of the photo excited germanium nanoparticles and charge transport. The current–voltage characteristics were recorded with a Keithley 2400 Source measurement unit and a Xenon Short Arc 80 W lamp was used as light source. The xenon lamp has a smooth spectrum in the visible from 300 until about 800 nm after which a range with sharp peaks and valleys dominate the spectrum. The spectrum is a good approximation of the solar spectrum. Monochromatic light was obtained by placing an Oriel Omni 300 monochromator between the lamp and solar cell. The light from the lamp was focused into an optical fiber which illuminated the solar cell.

3. Results and Discussion

Germanium nanoparticles were initially investigated by TEM, as shown in **Figure 1**, which demonstrated primarily monodispersed germanium nanoparticles with occasionally secondary adjacent nanoparticles. The diameters of the germanium nanoparticles were measured and resulted in a nanoparticle size distribution which could be successfully modeled with a lognormal distribution.[31,32] The inset plot of Figure 1 represents a statistical analysis of single and adjoined nanoparticle diameters with a lognormal fitting. Adjoined nanoparticles were
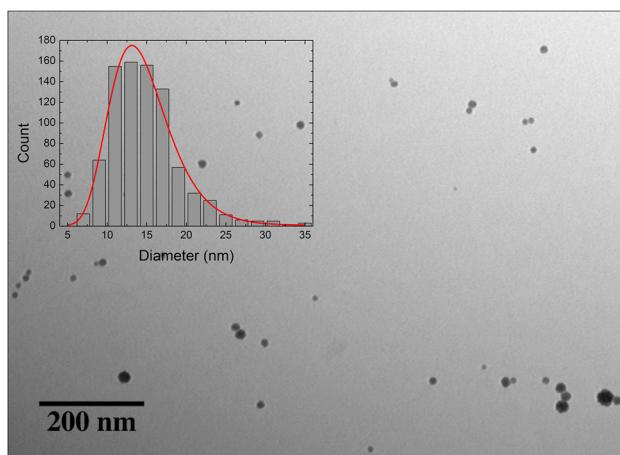

Figure 1. Germanium nanoparticles deposited on a holey carbon TEM grid for 10 min at an aggregation length of 30 mm. The inset plot is a statistical analysis of the 825 identified particles with a lognormal distribution (fit) with a mean diameter of 14 nm. A significant majority of the particles are within the quantum confinement regime.

rectified by taking negligibly overlapping spherical approximations. The mean diameter of 14 nm lies below germanium's large exciton Bohr radius of 24 nm, likely giving rise to a significant quantum confinement effect.

High resolution TEM (**Figure 2**A–C) images reveal the typical nano-porous "cauliflower" structure as recently found in silicon nanoparticles from the same apparatus[33] and similar techniques.[24] The "cauliflower" nanoparticles are aggregates of smaller germanium nanoparticles, likely of a quantum confined size. The quantum confinement may be affected or even lifted at the nanoparticle contact points, while quantum confinement remains present in the direction were particles are well
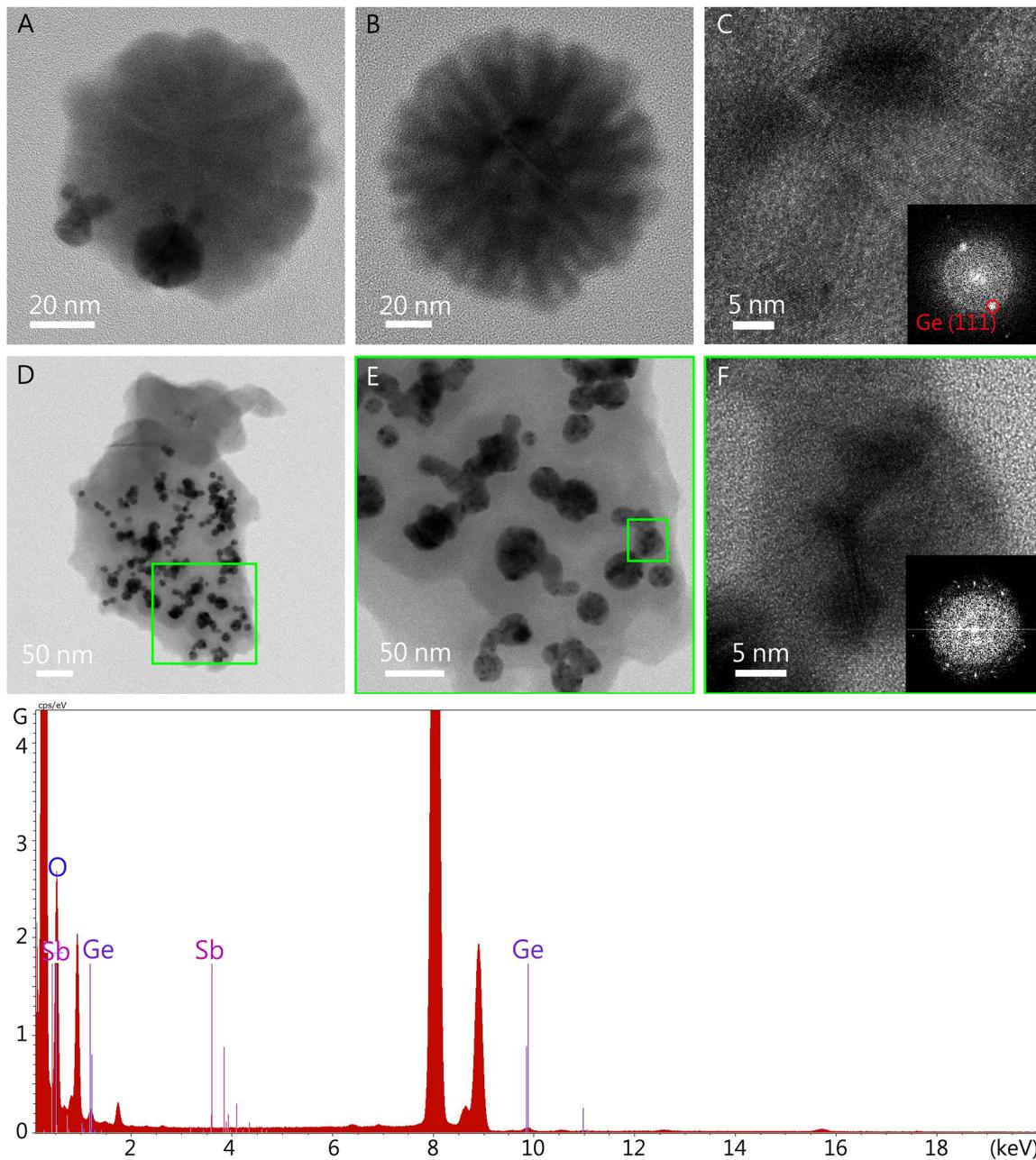

Figure 2. TEM images (recorded at a FEI Talos F200X) of Ge nanostructured particles of different morphologies. A) Larger "cauliflower" type germanium nanoparticle with smaller nanoparticles in close proximity. B) Another typical cauliflower nanoparticle with its center displayed in high resolution in panel (C), displaying Ge(111) atomic lattice fringes. D) An amorphous matrix with much smaller Ge nanoparticles embedded within. The area indicated with the green square is magnified in panel (E) where many particles displaying diffraction contrast, indicating polycrystallinity, are visible. F) High-resolution image of the area indicated with a green square in panel (E), showing nanodomains with Ge(111) atomic lattice fringes. The insets in panels (C) and (F) are Fourier transforms of these images, showing peaks belonging to Ge(111) lattice spacings. G) EDS spectrum of one particular area and deposition, showing a clear Ge and Sb signal.

separated. Figure 2D–F shows an example of very small germanium nanoparticles embedded in an amorphous germanium matrix. Occasionally, nanosheets and irregularly shaped particles were observed as well. As each TEM sample corresponds to different depositions, it is clear that the nanoparticle source produces a wide range of nanoparticle sizes, shapes and forms, which all together form the basis of the thicker layers deposited on the electrodes. It is very likely that pockets of crystalline, polycrystalline, and amorphous germanium coexist, in agreement with other work.[34] The areas of crystallinity are apparent from the (dark) diffraction contrast displayed by many of the particles in Figure 2, while high-resolution Ge(111) atomic lattice fringes are clearly visible in Figure 2C,E, as is also clear from the corresponding Fourier transforms (insets in Figure 2C,F).

Energy dispersive X-ray spectrometry (EDS, Figure 2G) analysis provided concentrations of 96 at% Ge, doped with 4 at% Sb. Sometimes the germanium particles consisted of 100% Ge. The large particles with smaller germanium nanoparticles embedded were composed of 80 at% Ge and 20 at% Sb. Again, the composition also has a wide range of values, resulting in a wide range of concentrations present in the thicker layers on the electrodes. Because of the high O background from the organic contaminations (due to pre-deposition dust), the O content in the Ge particles could not be quantified.

The germanium nanoparticle depositions on ITO resulted in three types of samples: thin (358 nm), medium (965 nm), and thick (8.9 μm) layers. The actual thickness was estimated by the optical absorption at 500 nm using the Lambert–Beer law and the optical absorption coefficient of a 20 nm thick germanium film.[35] Measuring the thickness by AFM is unfortunately not possible because the films are too thick (many monolayers) and the substrate is not exposed. The edge range is too large for the AFM scale. The analysis of AFM profiles provided information on the size distribution of the nanoparticles in the uppermost layer, which is nevertheless representative of the particles assembled in the bulk of the film. The mean height (diameter) of the particles was about 18 ± 3 nm. In the medium thick film also larger nanoparticles are visible, which are likely the "cauliflower" particles (**Figure 3**a) with an average size of 40 ± 12 nm. Glimpses of the underlying structure of smaller particles aggregating into larger particles can be seen in Figure 3b. Neither freestanding nanoparticle profiles nor the primary "cauliflower" structure could be imaged for the thick nanoparticle assembled film, due to the high-surface roughness and high density of nanoparticles. Instead, the height differences between large protruding nanoparticle features was measured, yielding an average size of 82 ± 34 nm.

UV–vis optical absorption spectroscopy on the three different types of samples resulted in different Tauc plots[36] for each electrode, in line with the difference in morphology (**Figure 4**). The Tauc plots were calculated from the optical absorption spectrum taking into account the Lambert–Beer law. Although the absorption lines are not straight, they could be fitted over the entire range with good accuracy.[37] This yielded a band gap of 1.02 ± 0.01 eV, 1.42 ± 0.02 eV, and 1.34 ± 0.01 eV for the thin, medium, and thick samples, respectively. This is strong evidence that although the germanium nanoparticle layers are composed of a wide range of sizes and shapes, small quantum confined
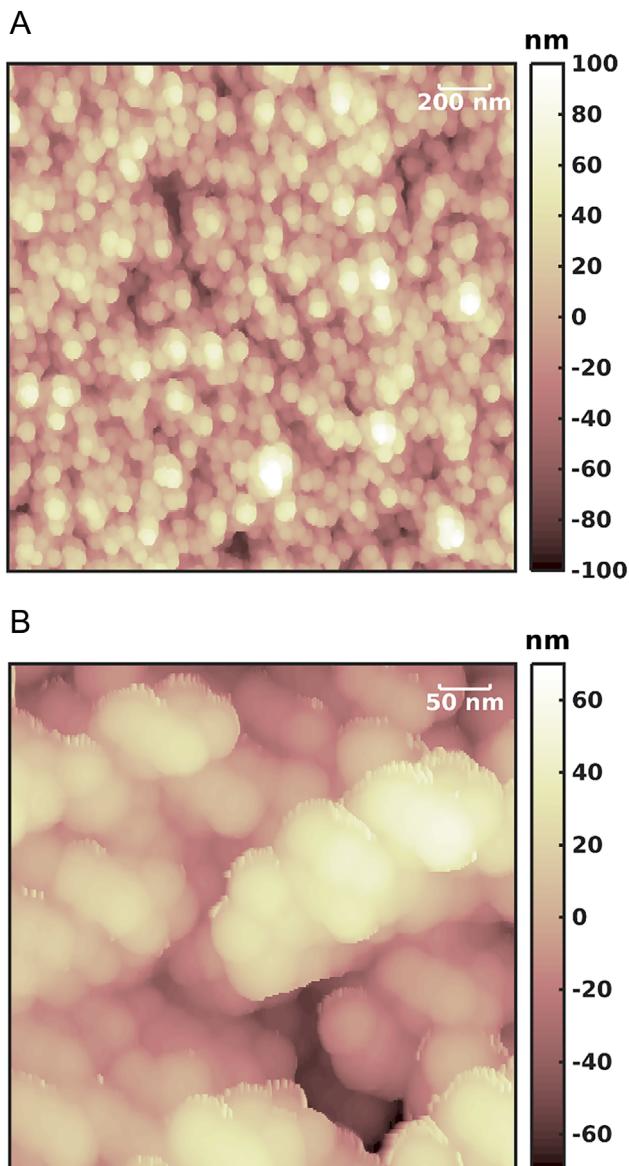
Figure 3. AFM images of germanium nanoparticles deposited with a magnetron sputtering gas aggregation nanoparticle source on ITO. A) Large nanoparticles are visible, likely of the typical "cauliflower" shape consisting of an aggregation of smaller germanium nanoparticles. B) A more detailed image clearly shows that the nanoparticles form a multi layered structure.

regions are present in abundance. Because the optical absorption may become a direct transition for quantum dots, its effect in the optical measurement may be enhanced as compared to the bulk germanium with an indirect optical transition, and it therefore dominates the spectrum. Although amorphous germanium is likely present in the nanoparticles and its band gap is 0.88 eV,[36] it is not enough to account for the measured band gaps exceeding 1 eV. A relation between the band gap and the layer thickness (surface morphology) is not possible due to the presence of small features hidden to AFM.
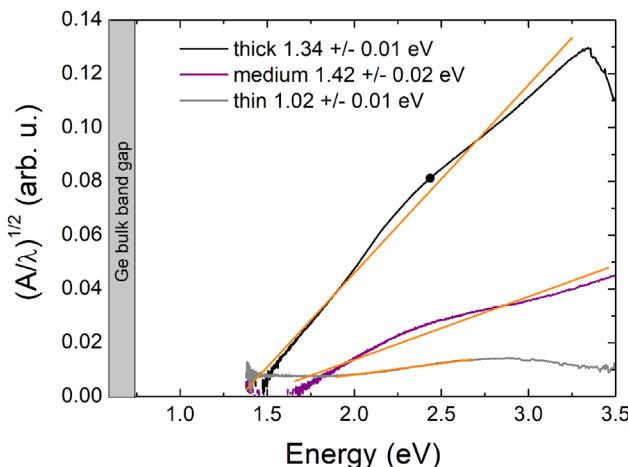
Figure 4. Tauc plots of the UV–vis absorption spectra of the thick, medium and thin germanium quantum dots on ITO/Glass. A fit (orange) through the region of interest provides the germanium quantum dot layer band gap.
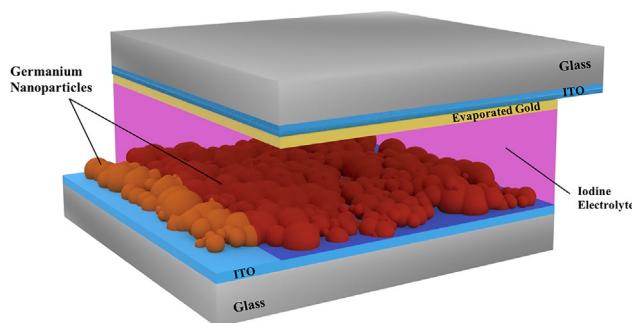

Figure 5. Schematic of the germanium Grätzel-type solar cell with the germanium quantum dots deposited by the magnetron sputtering nanoparticle source on top of the ITO. Between the cathode with a thin gold layer and the germanium quantum dots, a standard iodide/triiodide electrolyte was applied.

Previous quantum dot experiments found that the energy band structure of germanium is rich in several indirect and direct bandgap transitions between 0.6 and 6 eV.[38] The size-dependent quantum confinement in spherical germanium nanoparticles were calculated with effective mass approximations (EMA)[39] which were extended to contain Coulomb corrections.[40] Alternative empirical tight binding methods (ETBM)[41] and sp^3 tight binding models[42] were developed to compensate for EMA deficiencies. The simplified EMA for 3D germanium quantum dots experience weak, medium, and strong confinement.[26] The germanium nanoparticle minimum size of 6 nm in this work (Figure 1a) corresponds to a bandgap of 1.08 eV (using a bulk value of 0.66 eV[43]) while the mean diameter of 14 nm corresponds to a band gap close to that of the bulk value. Thick surface oxide shells can account for as much as 50% of the recorded size, creating significantly greater quantum confined non-oxidized germanium cores.[44,45] From the band gaps measured by the Tauc method, it can therefore be concluded that the observed germanium nanoparticles must contain smaller germanium crystallites to result in larger band gaps.

In order to measure the photoresponse of the germanium nanoparticle assembled layer, a Grätzel solar cell was fabricated with a counter electrode and electrolyte[28] as depicted in **Figure 5**. The advantage of a Grätzel solar cell is its relatively simple construction, avoiding the deposition of high-quality layers with well-tuned energy levels. In the dye sensitized solar cell (Grätzel cell), photons are absorbed into a molecular photosensitive dye covalently bonded to the surface of a thin film of TiO_2 nanoparticles. Excited electrons in photosensitizers are injected into the conduction band of the semiconductor – flowing through the back

contact of the cell. The oxidized dye is replenished through electron transfer from the redox in an electrolyte solution, which is in turn replenished by the counter electrode. In the germanium quantum dot solar cell the germanium nanoparticles act as the photosensitive dye and the semiconductor at the same time. The photo excited electron in the germanium particles moves through the nanoparticle network toward the ITO electrode, where it delivers a potential difference with respect to the cathode. The regeneration of the germanium quantum dots is provided by I^-, which injects electrons into the valence band. Therefore, the electrolyte redox potential should be aligned with the valence band of the germanium quantum dots. Although many other auxiliary reactions are present, in **Figure 6** the two most relevant energy
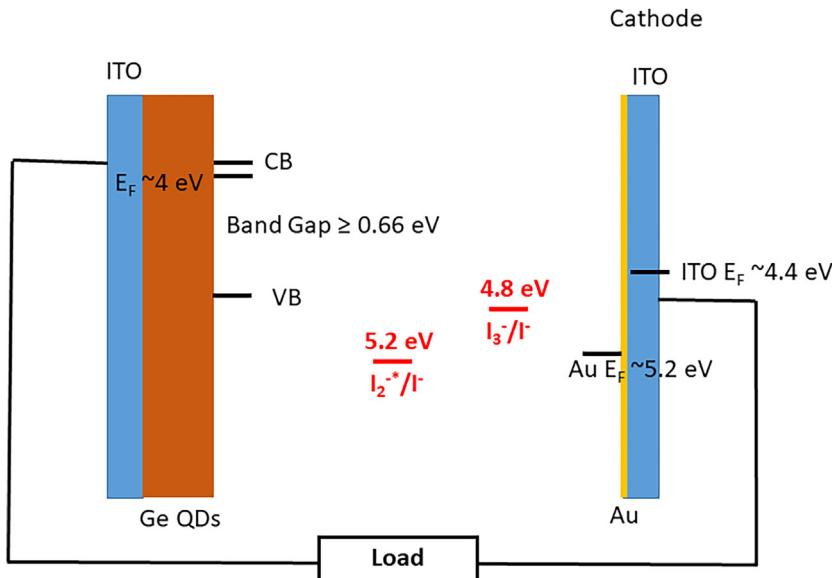

Figure 6. Schematic diagram depicting the germanium quantum dot solar cell electrodes, the Fermi energy levels, the germanium band gap, and the relevant I^-/I_3^- redox couple energy levels (red). The electrons promoted to the conduction band of the germanium quantum dots provide a voltage and are transported to the cathode. At the cathode surface the electrons are transferred to the I^-/I_3^- redox couple, after which the electrons are injected into the valence band of the germanium quantum dot.

levels of the regenerative cycle are shown (red). The electron injection into the germanium valence band depends on the degree of quantum confinement, which shifts the valence band level. The energy levels depicted in Figure 6 are taken from the literature.[25,46–48]

In **Figure 7**a, the photo generated power as a function of voltage is shown when the solar cell is illuminated with white light. The slow response time required sufficient time for the performance characterization.[49,50] The distinct difference between the solar cell with germanium quantum dots and the

Figure 7. A) Solar cell current–voltage (*I–V*) curve response of layered samples and the control sample (black) under the average white light intensity of 556 W m^{-2}. The solar cell with germanium particles has a much stronger response to light than the control cell, confirming the photo activity of the germanium quantum dots. B) Spectral response curves for the thin (green) medium (red) and thick (blue) germanium quantum dot solar cells. The black curve is the control measurement without germanium quantum dots. The difference in EQE can be explained by the difference in thickness: the more germanium quantum dots are present, the more photons are converted to electricity. The high EQE response below 450 nm is likely the result of a much larger band gap than crystalline or amorphous germanium. The solar cells were illuminated through the gold layer (solid) and through the germanium layer (dashed).

control solar cell without nanoparticles confirms the photo-activity of the germanium quantum dots. The open circuit potential is about 0.08 V, which is much lower as compared to the band gap of 0.66 eV. There are several mechanisms which can affect the open circuit potential, of which the very high abundance of defects, both at the surface and inside the germanium quantum dots, is the most likely cause. Moreover, on the oxide layer at the surface of the germanium quantum dots a considerable potential drop is expected due to its high electric resistance. By taking an oxide layer of several nm thick, a surface area of about 0.5 cm^2 and a resistivity of about $10^8 \, \Omega \, m$[51] a series resistance of the order of 10 kΩ is reasonable. Considering that the resistance of this type of solar cell is of the order of several Ohm, this should lead to a voltage reduction in the order of a thousand or more. Since the actual voltage reduction is of the order of 10, it is clear that very likely, the electrons are able to tunnel through the thin oxide layer, lowering the overall electrical resistance. The efficiencies of the thin, medium, and thick solar cells are 1.6×10^{-5}, 5.4×10^{-5}, and 0.011%, respectively. When the oxide layer can be avoided, the latter percentage could be easily multiplied by a factor of 100 (factor of 10 in voltage and factor of 10 in current), resulting in an efficiency of about 1%.

The spectral response of the germanium quantum dot solar cell in Figure 7b also shows a strong difference between the solar cells with germanium nanoparticles and without (control experiment). It is also clear that the solar cell with the thickest germanium quantum dot layer, provides the largest external quantum efficiency (EQE) due to the larger amount of photo converters. Between 800 and 400 nm the photo response is rather constant after which the EQE strongly increases (below 400 nm). Since the band gap of 0.66 eV corresponds to 1879 nm, a jump in photo response at 400 nm can only be explained by a germanium nanoparticle band gap increase toward about 3.1 eV. This energy corresponds to germanium quantum dots with a diameter of about 2 nm according to calculations by Niquet et al.[42] Such small germanium nanoparticles could be the constituents of the larger nanoparticles, such as the "cauliflower" shaped particles, maintaining a certain amount of quantum confinement. However, thin Germanium layers of 0.4 and 1.5 nm previously exhibited bandgaps in excess of 1.3 eV, which were likely a result of interfacial contributions to carrier confinement.[52] Such interfacial effects could also significantly affect the band gaps observed here. Alternatively, electrons promoted from the valence band by photons exceeding about 3.1 eV may be more efficiently transported by an intermediate conducting level in germanium or ITO. Although AFM and TEM images suggest that the conditions for quantum confinement are plausibly met, the extent of it is difficult to establish, due to other contributing effects. The high density of transitions and the nanoparticle size dispersion likely contribute to a wide spread of overlapping bandgap availabilities.

Figure 7b shows that when the solar cell is illuminated from the gold layer side, the photo response is considerably higher than when the solar cell is illuminated from the germanium nanoparticle side, particularly for the thick germanium quantum dot solar cell. Because very little light reaches the germanium particles at the electrolyte side when illuminated from the germanium nanoparticle side, this suggests that the transport of
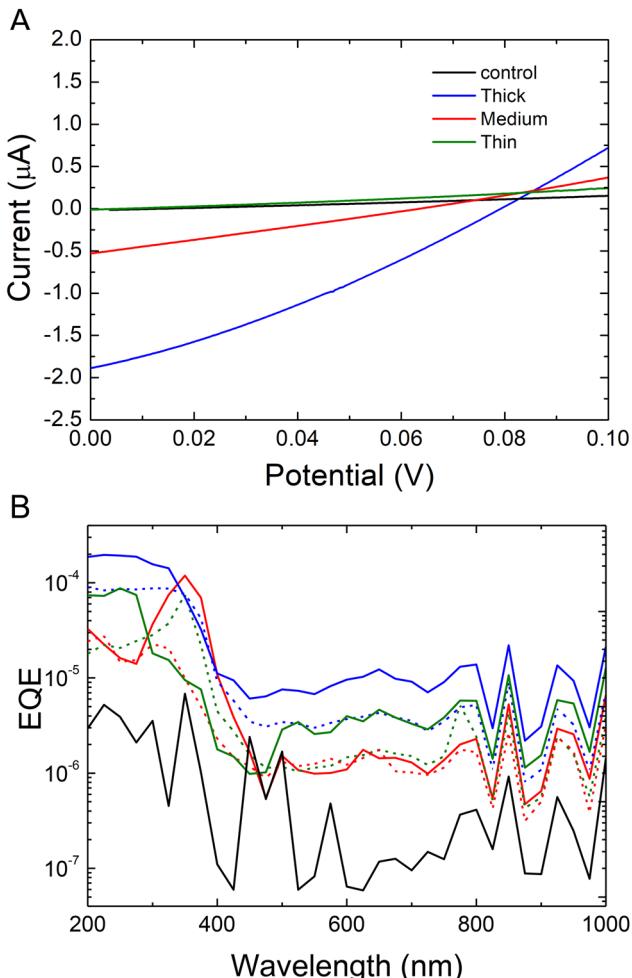
ADVANCED
SCIENCE NEWS
www.advancedsciencenews.com

physica
pss
status
solidi
a
www.pss-a.com

charge carriers inside the germanium nanoparticle network is limited, likely due to an abundance of defects.

The peak value of the photo response of the thin solar cell around 330 nm could be the result of a transition to a distinct energy level. Because quantum confinement not only affects the band gap, but also introduces discrete intermediate energy levels. Since the thin solar cell photo response is averaged over less particles, an abundance of one particular germanium quantum dot size may allow the appearance of such a discrete line.

Future experiments could involve quadrupole[53] or time of flight[54,55] mass selectors to obtain narrow size dispersions to increase the control over the band gap for each particle. Because mass selection results in a much smaller amount of nanoparticles, the possibility to deposit sufficiently thick quantum dot layers remains to be investigated.

4. Conclusions

In summary, for the first time, to the best of our knowledge, a proof of principle germanium quantum dot solar cell has been fabricated, in which the quantum dots were produced using a (magnetron sputtering) gas aggregation nanoparticle source. Although the germanium quantum dot solar cell had a very low efficiency, a clear spectral response suggests quantum confinement, which is supported by the TEM and UV–vis spectroscopy experiments. Future work should focus on combining the germanium (or silicon) nanoparticles from the gas aggregation cluster source with semiconductor and conducting thin films to prevent oxidation and provide well leveled p–n junctions. In principle, a full quantum dot solar cell constructed with a gas aggregation nanoparticle source could be fabricated in such a way. This work demonstrates for the first time the feasibility of using an industrially interesting gas aggregation nanoparticle sources for fabricating quantum dot based solar cells, paving the way for higher efficiency sustainable quantum dot solar cells.

Conflict of Interest

The authors have declared no conflict of interest.

[1] C. E. Nebel, S. Christiansen, H. P. Strunk, B. Dahlheimer, U. Karrer, M. Stutzmann, *Phys. Status Solidi A* **1998**, *166*, 667.
[2] A. Nozik, *Physica E* **2002**, *14*, 115.
[3] A. P. Alivisatos, *J. Phys. Chem.* **1996**, *100*, 13226.
[4] D. C. Law, R. R. King, H. Yoon, M. J. Archer, A. Boca, C. M. Fetzer, S. Mesropian, T. Isshiki, M. Haddad, K. M. Edmondson, D. Bhusari, J. Yen, R. A. Sherif, H. A. Atwater, N. H. Karam, *Sol. Enrgy Mater. Sol. Cells* **2010**, *94*, 1314.
[5] C. B. Murray, C. R. Kagan, M. G. Bawendi, *Annu. Rev. Mater. Sci.* **2000**, *30*, 545.
[6] G. E. Jabbour, D. Doderer, *Nat. Photonics* **2010**, *4*, 604.
[7] X. Dai, Y. Deng, X. Peng, Y. Jin, *Adv. Mater.* **2017**, *29*, 1607022.
[8] J. Xu, O. Voznyy, M. Liu, A. R. Kirmani, G. Walters, R. Munir, M. Abdelsamie, A. H. Proppe, A. Sarkar, F. P. García de Arquer, M. Wei, B. Sun, M. Liu, O. Ouellette, R. Quintero-Bermudez, J. Li, J. Fan, L. Quan, P. Todorovic, H. Tan, S. Hoogland, S. O. Kelley, M. Stefik, A. Amassian, E. H. Sargent, *Nat. Nanotechnol.* **2018**, *13*, 456.
[9] G. H. Carey, A. L. Abdelhady, Z. Ning, S. M. Thon, O. M. Bakr, E. H. Sargent, *Chem. Rev.* **2015**, *115*, 12732.
[10] G. Conibeer, *Mater. Today* **2007**, *10*, 42.
[11] A. G. Cullis, L. T. Canham, *Nature* **1991**, *353*, 335.
[12] W. D. A. M. de Boer, D. Timmerman, K. Dohnalova, I. N. Yassievich, H. Zhang, W. J. Buma, T. Gregorkiewicz, *Nat. Nanotechnol.* **2010**, *5*, 878.
[13] A. A. Prokofiev, A. S. Moskalenko, I. N. Yassievich, W. D. A. M. de Boer, D. Timmerman, H. Zhang, W. J. Buma, T. Gregorkiewicz, *JETP Lett.* **2010**, *90*, 758.
[14] C. Delerue, G. Allan, M. Lannoo, *J. Lumin.* **1998**, *80*, 65.
[15] G. Ledoux, O. Guillois, D. Porterat, C. Reynaud, F. Huisken, B. Kohn, V. Paillard, *Phys. Rev. B* **2000**, *62*, 15942.
[16] S. Takeoka, M. Fujii, S. Hayashi, *Phys. Rev. B* **2000**, *62*, 16820.
[17] E. Tekin, P. J. Smith, U. S. Schubert, *Soft Matter* **2008**, *4*, 703.
[18] W. L. Wilson, P. F. Szajowski, L. E. Brus, *Science* **1993**, *262*, 1242.
[19] D. Timmerman, J. Valenta, K. Dohnalova, W. D. A. M. de Boer, T. Gregorkiewicz, *Nat. Nanotechnol.* **2011**, *6*, 710.
[20] M. T. Trinh, R. Limpens, W. D. A. M. de Boer, J. M. Schins, L. D. A. Siebbeles, T. Gregorkiewicz, *Nat. Photonics* **2012**, *6*, 316.
[21] G. Conibeer, M. Green, R. Corkish, Y. Cho, E.-C. Cho, C.-W. Jiang, T. Fangsuwannarak, E. Pink, Y. Huang, T. Puzzer, T. Trupke, B. Richards, A. Shalav, K. Lin, *Thin Solid Films* **2006**, *511*, 654.
[22] T. Shimizu-Iwayama, N. Kurumado, D. E. Hole, P. D. Townsend, *J. Appl. Phys.* **1998**, *83*, 6018.
[23] M. Di Vece, *KONA Powder Part. J.* **2018**. https://doi.org/10.14356/kona.2019005
[24] W. Tang, J. J. Eilers, M. A. van Huis, D. Wang, R. E. I. Schropp, M. Di Vece, *J. Phys. Chem. C* **2015**, *119*, 11042.
[25] E. S. M. Goh, T. P. Chen, C. Q. Sun, Y. C. Liu, *J. Appl. Phys.* **2010**, *107*, 024305.
[26] E. G. Barbagiovanni, D. J. Lockwood, P. J. Simpson, L. V. Goncharova, *Appl. Phys. Rev.* **2014**, *1*, 011302.
[27] D. E. Aspnes, A. A. Studna, *Phys. Rev. B* **1983**, *27*, 985.
[28] B. O'Regan, M. Grätzel, *Nature* **1991**, *353*, 737.
[29] H. Haberland, M. Mall, M. Moseler, Y. Qiang, T. Reiners, Y. Thurner, *J. Vac. Sci. Technol.* **1994**, *12*, 2925.
[30] H. Haberland, M. Karrais, M. Mall, Y. Thurner, *J. Vac. Sci. Technol.* **1992**, *10*, 3266.

[31] J. Söderlund, L. B. Kiss, G. A. Niklasson, C. G. Granqvist, *Phys. Rev. Lett.* **1998**, *80*, 2386.

[32] J. G. Couillard, *Ph.D. Thesis*, Nanostructures for Group IV Optoelectronics, Cornell University, **1996**.

[33] A. Mohan, M. Kaiser, M. A. Verheijen, R. E. I. Schropp, J. K. Rath, *J. Cryst. Growth* **2017**, *467*, 137.

[34] H.-S. Li, F. Qiu, Z.-H. Xin, R.-F. Wang, J. Yang, J. Zhang, C. Wang, Y. Yang, *Jpn. J. Appl. Phys.* **2016**, *55*, 061302.

[35] A. Ciesielski, L. Skowronski, W. Pacuski, T. Szoplik, *Mater. Sci. Semicond. Process.* **2018**, *81*, 64.

[36] J. Tauc, R. Grigorovici, A. Vancu, *Phys. Status Solidi B* **1966**, *15*, 627.

[37] N. Ghobadi, *Int. Nano Lett.* **2013**, *3*, 2.

[38] J. R. Heath, J. J. Shiang, A. P. Alivisatos, *J. Chem. Phys.* **1994**, *101*, 1607.

[39] A. Efros, A. L. Efros, *Sov. Phys. Semicond.* **1982**, *16*, 772.

[40] Y. Kayanuma, *Phys. Rev. B* **1988**, *38*, 9797.

[41] Y. Wang, N. Herron, *J. Phys. Chem.* **1991**, *95*, 525.

[42] Y. M. Niquet, G. Allan, C. Delerue, M. Lannoo, *Appl. Phys. Lett.* **2000**, *77*, 1182.

[43] B. Streetman, S. Banerjee, *Solid State Electronic Devices*, Pearson, London **2015**.

[44] M. Han, Y. Gong, J. Ma, F. Liu, G. Wang, *Jpn. J. Appl. Phys.* **1995**, *34*, 49.

[45] S. Hayashi, S. Tanimoto, M. Fujii, K. Yamamoto, *Superlattices Microstruct.* **1990**, *8*, 13.

[46] Y. Park, V. Choong, Y. Gao, B. R. Hsieh, C. W. Tang, *Appl. Phys. Lett.* **1996**, *68*, 2699.

[47] K. C. D. Robson, P. G. Bomben, C. P. Berlinguette, *Dalton Trans.* **2012**, *41*, 7814.

[48] N. Tallaj, M. Buyle-Bodin, *Surf. Sci.* **1977**, *69*, 428.

[49] M. Falconieri, G. Duva, S. Gagliardi, *J. Phys. D: Appl. Phys.* **2014**, *47*, 495102.

[50] Y. Hishikawa, M. Yanagida, N. Koide, in *Conf. Record of the Thirty-First IEEE Photovoltaic Specialists Conference, 2005* **2005**, pp. 67–70.

[51] C. V. Ramana, I. B. Troitskaia, S. A. Gromilov, V. V. Atuchin, *Ceram. Int.* **2012**, *38*, 5251.

[52] G. H. Shih, C. G. Allen, B. G. P. Potter Jr., *Nanotechnology* **2012**, *23*, 075203.

[53] P. Wolfgang, *Steinwedel Helmut, zna* **2014**, *8*, 448.

[54] W. A. de Heer, P. Milani, *Rev. Sci. Instrum.* **1991**, *62*, 670.

[55] B. von Issendorff, R. E. Palmer, *Rev. Sci. Instrum.* **1999**, *70*, 4497.